# Surface flow visualization of a side-mounted NACA 0012 airfoil in a transonic Ludwieg tube

**F.K. Lu, E.M. Braun, and T.S. Balcazar**

## 1 Introduction

Transonic testing is confronted with numerous challenges such as the need to match fullscale Mach and Reynolds numbers, as well as to ensure interference-free flow. Various methods such as porous [1] or adaptive walls [2, 3] are used for the latter. More modern methods involve a combination of "corrections" using numerical simulations [4]. While cryogenic tunnels are used for industrial purposes [5, 6], small Ludwieg tube tunnels have an important role in wind tunnel testing [7].

The Ludwieg tube falls within the family of impulse test facilities where its operation depends on unsteady waves propagating in tubes [8]. It was originally proposed for transonic testing with its requirement to match fullscale Mach and Reynolds numbers. In addition, the unsteady expansion damps out flow unsteadiness to produce a "quiet" flow. This quiet feature has been exploited successfully for transition studies in a Mach 5 Ludwieg tube [9].

The Ludwieg tube at the University of Texas at Arlington, known as the **HI**gh **R**eynolds number **T**ransonic tunnel (HIRT), was originally installed at the Arnold Engineering Development Center as a $1/13^{th}$ scale model of a larger facility that was never built [10]. The Ludwieg tube was decommissioned from AEDC in 1976 and reinstalled at UTA in 1978. It had been used for studying rotorcraft blade/vortex interactions, advanced fighter wings and advanced rotortip shapes. It was refurbished in 2010. This paper reports the development of surface flow visualization in this facility using a NACA0012 wingtip.

*Aerodynamics Research Center, Mechanical and Aerospace Engineering Department, University of Texas at Arlington, Arlington, Texas 76019, USA*

# 2 Experiment

## *2.1 Facility Characteristics*

A schematic of the HIRT is shown in Fig. 1. The tunnel consists of a charge tube, convergent nozzle, test section, ejector flap section, diffuser and a sliding sleeve valve (SSV). The circular charge tube transitions to a rectangular test section via a nozzle with a contraction ratio of 2.27. The test section measures 184.9 mm high, 232.2 mm wide and 635 mm long.

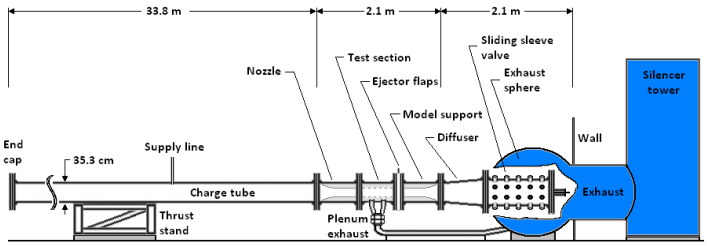


**Fig. 1** Elevation view of HIRT.

The porous wall, test section allows test models of large chord to be used. The porous wall requires that the test section be surrounded by a plenum chamber. The porous walls consist of two stacked plates with 30 deg inclined holes and a tapered porosity pattern in the upstream one third of the test section length. The holes are 3.04 mm apart. The porosity can be varied manually from 3.5 to 10 percent by moving one plate relative to the other.

While the contraction ratio is fixed, the test section Mach number can be changed by adjusting the exhaust flow through opening a certain number of the 27 ports in the SSV. The Mach number ranges from 0.5–1.2. The high pressure of the charge tube provides an independent Reynolds number variation of $40–400 \times 10^6$/m.

Instrumentation is located in the charge tube, plenum chamber, and test section. A thermocouple and a pitot probe are mounted along the wall of the charge tube to measure flow conditions prior to the nozzle. The total pressure measurement is used to calculate the Mach number using

$$M = \sqrt{\left(\frac{2}{\gamma - 1}\right)\left[\left(\frac{p_t}{p_s}\right)^{(\gamma-1)/\gamma} - 1\right]} \tag{1}$$

where $p_s$ and $p_t$ are the static and total pressure measured in the test section.

A NACA 0012 model was fit onto a plug with a diameter of slightly less than 76 mm which connects to a sidewall force balance, Fig. 2. The airfoil has a 50.8 mm chord and a 101.6 mm span along with a rounded tip with the same NACA

0012 profile. The force balance is free to rotate, allowing for the angle of attack to be adjusted. Due to the high force exerted on the model during the run, a small gap between the disk and the wall is required to allow the balance to flex without interfering with measurements.

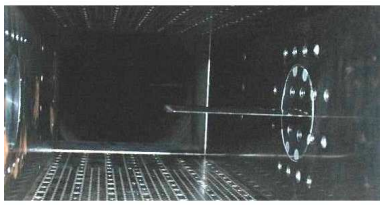

**Fig. 2** Test section showing the semispan wing with a NACA 0012 profile.

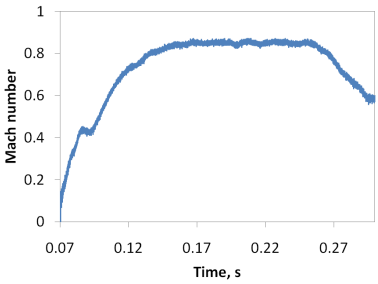


**Fig. 3** Typical performance at a Mach 0.85 condition.

## *2.2 Test Conditions*

The charge tube is rated to 45 atm. When the SSV is opened rapidly, it generates an expansion wave which travels upstream into the charge tube that allows for a theoretical, steady test time of 185 ms. The actual steady test time is about 120 ms due to the nonideal opening of the SSV. The tests were conducted at Mach 0.85 $\pm$ 0.015 (95% confidence) with a Reynolds number of $59 \times 10^6$/m.

## *2.3 Surface Flow Visualization*

Two surface flow visualization techniques were utilized. The first applies oil dots along the span of the wing at different chord locations. This oil dot method is well established [11]. However, one potential difficulty is that it may be difficult to distinguish which trace was made during the start-up process and which were made while running at the test conditions [12]. For the Ludwieg tube operation, it is expected that the short start-up time may cause minimal effects on the flow visualization. The mixture consists of oil-based paint and SAE-85W140 gear oil. The paint/oil ratio was about 2:3 for both colors chosen namely, blue and yellow. The paint was applied using a thin wire. Surface oil flow visualization was also applied. Recent work utilized ground fluorescent chalk. The chalk particles were passed through a 100 $\mu$m filter prior to mixing with a carrier of light oil. To produce satisfactory results, the mixture was applied as a film with a soft brush over the entire surface of the airfoil

prior to a test. The fluorescence was excited by “blacklight” to produce bright and highly resolved pictures.

# 3 Results

## *3.1 Oil Dot Visualization*

Figure 4(a) shows that a row of blue dots followed by a row of yellow dots was placed across the span of the wing. The figure shows the shadow from the mounting plug. An example of the oil dot visualization is shown in Fig. 4(b). The most evident features in this figure are the inward turning due to the pressure differences on the top and bottom of the wing. In addition, the mixing of the blue and yellow colors indicates flow reversal close to the trailing edge due to separation. Although separation can be identified at particular locations, the short run time limits the oil dot method from making a complete trace along the entire wing. This creates difficulty in identifying the separation line. Besides flow reversal and inward turning, there are no other evident features in the results using this technique. A disadvantage of this technique is that it is mostly limited to visualizing only inward turning and separation.

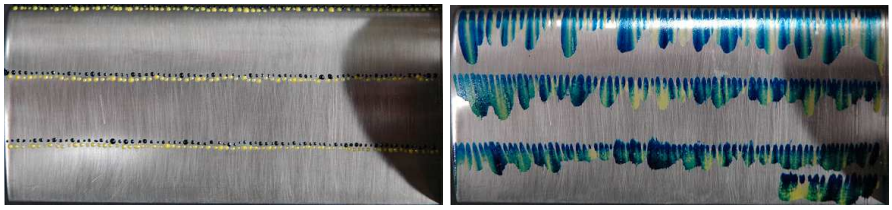

(a) Before a test.

(b) Wing at 6 deg AOA, Mach 0.85, $Re = 3.24 \times 10^6$.

**Fig. 4** SFV results with oil flow dots.

## *3.2 Oil Flow Visualization*

Images taken for 0 and 6 degree AOA tests are shown along with sketches of the surface characteristics. For the 0 degree result, shock-induced boundary layer separation is clearly visible at about 60 percent chord. At that point, the streaks left by the chalk particles are no longer visible and the surface appears blurred when compared to the rest of the airfoil. This location is similar to two-dimensional results obtained with $M$ = 0.84–0.86 and $Re$ = 3–4 million [14, 15]. Several other features

are visible. Near to the leading edge of the airfoil, transition appears to be marked with a line that is uniform across almost all of the airfoil. Transition causes a rise in shear stress, which affects the distribution of luminescent particles. After the transition point, a dark band appears around $x/c = 0.25$. This is visible for all fluorescent SFV experiments and could be related to weak waves over the airfoil. This could be a transient effect, and it appears too far upstream of the separation location to be related to the upstream influence. The upstream influence appears just before the separation and is more visible in the middle of the airfoil.

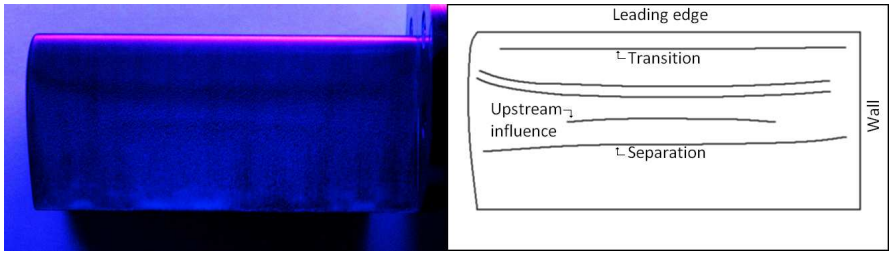


**Fig. 5** Fluorescent surface oil flow visualization of wing at zero incidence, Mach 0.85 $\pm 0.015$, and $Re = 3.24 \times 10^6$.

Figure 6 shows a photograph and sketch of a Mach 0.87 test with the airfoil at a 6 degree AOA. Here, all of the surface flow characteristics move forward as anticipated. Inward turning that occurs due to the positive AOA is also visible in this case.

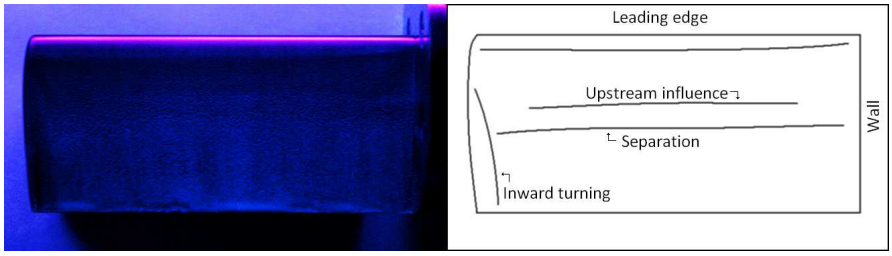


**Fig. 6** Fluorescent surface oil flow visualization of the airfoil at a 6 deg AOA, Mach 0.87, and $Re = 3.27 \times 10^6$.

## 4 Conclusions

The potential use of surface flow visualization in a short-duration Ludwieg tube was explored. Two techniques were applied, namely, oil dot and surface oil flow. The lat-

ter appears to be more suitable, especially in producing high resolution images. The images were enhanced using fluorescent pigments. Surface oil flow visualization appeared successful in locating the shock-induced separation.

**Acknowledgements** The authors would like to thank Professor Joseph Schetz (Virginia Polytechnic Institute & State University) for the initial motivation and financial support to begin refurbishing the tunnel. Thania Balcazar was supported by a scholarship from the University of Texas at Arlington Undergraduate Research-based Achievement for Science, Technology, Engineering and Mathematics. The authors acknowledge the help of Duong Tran who was supported by the University of Texas at Arlington "I Engage Mentoring Program."

## References

1. Knechtel ED (1959) Experimental investigation at transonic speeds of pressure distributions over wedge and circular-arc airfoil sections and evaluation of perforated-wall. NASA-TN-D-15
2. Sears WR, Erickson JC, Jr (1988) Adaptive wind tunnels. Ann Rev Fluid Mech 20:17–32.
3. Meyer O, Nitsche W (2004) Update on progress in adaptive wind tunnel wall technology. Prog Aerosp Sci 40(3):119–141.
4. Bosnyakov S, Kursakov I, Lysenkov A, Matyash S, Mikhailov S, Vlasenko V, Quest J (2008) Computational tools for supporting the testing of civil aircraft configurations in wind tunnels. Prog Aerosp Sci 44(2):67–120.
5. Goodyer MJ (1992) The cryogenic wind tunnel. Prog Aerosp Sci 29(3):193–220.
6. Rudnik R, Germain E (2009) Reynolds number scaling effects on the European High-Lift Project configurations. J Aircraft 46(4):1140–1151.
7. Squire LC (1998) A review of the role of some small high-speed wind tunnels in aeronautical research. Prog Aerosp Sci 34(3–4):107–166.
8. Ludwieg H (1957) Tube wind-tunnel: a special type of blowdown tunnel. AGARD-R-143.
9. Schneider SP, Haven CE (1975) Quiet-flow Ludwieg tube for high-speed transition research. AIAA J 33(4):688–693.
10. Starr RF (1975) Experiments to assess the influence of changes in the tunnel wall boundary layer on transonic wall crossflow characteristics. AEDC-TR-75-97.
11. Merzkirch W (1987) Flow Visualization, Academic, Orlando, Florida, 1987.
12. Lepicovsky J (2008) Investigation of flow separation in a transonic-fan linear cascade using visualization methods. Exp Fluids 44(6):939–949.
13. Pierce AJ, Lu FK, Bryant DS, Shih Y (2010) New developments in surface oil flow visualization. AIAA Paper 2010–4353.
14. Harris CD (1981) Two-dimensional aerodynamic characteristics of the NACA 0012 airfoil in the Langley 8-foot Transonic Pressure Tunnel. NASA TM–81927.
15. Mineck RE, Hartwich PM (1996) Effect of full-chord porosity on aerodynamic characteristics of the NACA 0012 airfoil. NASA TP–3591.